December 1991

M91-113

T. J. Elkins
J. Providakes

ESD/RADC OTH RADAR SYMPOSIUM, 5–7 NOVEMBER 1991, HANSCOM AFB

HFRAD HINDCAST: AN OTH-B RADAR AND MODEL COMPARISON STUDY

MITRE
Bedford, Massachusetts

December 1991

M91-113

T. J. Elkins
J. Providakes

ESD/RADC OTH
RADAR SYMPOSIUM,
5–7 NOVEMBER 1991,
HANSCOM AFB

HFRAD HINDCAST: AN OTH-B RADAR AND MODEL COMPARISON STUDY

CONTRACT SPONSOR ESD
CONTRACT NO. F19628-89-C-0001
PROJECT NO. 4141J
DEPT. D085

MITRE

The MITRE Corporation
Bedford, Massachusetts

ABSTRACT

Hindcast analysis of OTH radar data differs from purely predictive (or forecast) analysis in that it is made "after the fact" of radar measurement, permitting the removal of a substantial part of the random variability inherent in forecasting radar performance. In this paper, hindcast analysis is used to verify the performance of the MITRE OTH radar performance model, HFRAD. Data was collected during November and December of 1990 with the AN/FPS-118 East Coast Radar System (ECRS), and during January and February of 1991 with the West Coast Radar System (WCRS). This data was analyzed and compared to hindcast estimates of performance using a new version (V507g) of HFRAD that incorporates a new and improved, clutter model. Performance was analyzed in terms of target signal-to-noise ratio (SNR), both for the aggregate data set and for the data as a function of azimuth (because of its location near the auroral oval, the ECRS is known to exhibit a strong dependence of performance on azimuth). In addition, these internal model components were analyzed in the same way: subclutter visibility (SCV), surface clutter peak, background noise (i.e., noise measured with transmitter operating), noise measured with transmitter off (ambient noise), and the ratio of background noise to ambient noise. As anticipated, the comparison is generally in good agreement, although notable discrepancies still exist, particularly near the auroral oval. Suggestions for further improvements to HFRAD are presented.

ESD/RADC OTH RADAR SYMPOSIUM
5-7 NOVEMBER 1991
HANSCOM AFB

HFRAD HINDCAST: AN OTH-B RADAR AND MODEL COMPARISON STUDY

T. J. Elkins
J. F. Providakes

The MITRE Corporation
Bedford, Massachusetts 01730

The performance of Over-the Horizon (OTH) radar is strongly dependent on ionospheric propagation and, by extension, on ionospheric structure as well. The ionosphere is a highly dynamic propagation medium that exhibits both deterministic and random components of variability. In predicting the performance of OTH radars, it is first necessary to predict ionospheric structure and then compute the propagation modes and losses experienced by the radar energy. Ionospheric climatological models exist for the deterministic component, but the random component must be modeled in statistical terms. This creates difficulties in testing other components of radar performance models, since several of these have strong frequency dependences; a prime example is radar clutter magnitude, which has an inverse cube frequency dependence.

One way to avoid that difficulty is to compare OTH radar data with a model in which the random component has been removed to the extent possible by measuring the ionospheric parameters prevailing during the measurement and using the actual radar frequency, rather than the frequency that would be predicted by the propagation model. This technique is known as "hindcasting," as opposed to the purely predictive technique. This paper describes a hindcast analysis designed to test the accuracy of the MITRE OTH radar performance prediction program, HFRAD, using data collected with the U.S. Air Force AN/FPS-118 radar.

Hindcast consists of running HFRAD after the fact (e.g., after a radar measurement has been made) with the actual values of radar frequency and waveforms, sunspot number (SSN), magnetic activity (Kp), and ionospheric layer parameters. Using the actual ionospheric parameters allows the propagation mode used by HFRAD to agree with that measured during the data collection period. However, the removal of uncertainty in the operation frequency, system sensitivity parameters, and propagation mode does not completely eliminate all the model variances; for example, as will be shown later, there is still a substantial uncertainty in the propagation loss.

HFRAD contains several major model components that are used in computing the signal-to-noise ratio (SNR) for a given radar cross section (RCS). Figure 1 illustrates the major components that are involved in the OTH radar range equation. The major model components include the following: (1) radar equipment model (coherent integration time, τ; signal processing loss, L_{sp}; transmit antenna gain, G_t; receive antenna directivity, D_R; transmit power, P_t); (2) propagation model (propagation mode to target, 1F2, 1F1, etc.; slant range, R; maximum usable frequency (MUF); focusing factor, F; ionospheric layer parameters, foF2, foF1, foE, foEs; sporadic-E loss, L_{Es}; ionospheric D-region non-deviative absorption, L_D; auroral absorption, L_{AUR}); (3) noise model (atmospheric, man-made, and system noise, N); (4) clutter model (only outer Doppler clutter, C); and (5) radar cross section (target, σ_t) and surface reflectivity (σ_o).

Some of the above OTH radar model components can be directly measured, others must be inferred from a combination of measurements, and some are not available; for example, in the radar range equation

$$SNR = \frac{P_t G_t D_R \lambda^2 \tau \sigma F}{(4p)^3 R^4 L_T (N + C)} , \qquad (1)$$

where $L_T = L_{sp} + L_D + L_{AUR} + L_{Es}$

$$SNR = \frac{P_t G_t D_R \lambda^2 \tau \sigma F}{(4\pi)^3 R^4 L (N + C)}$$

$$L = L_D + L_{AUR} + L_{ES}$$

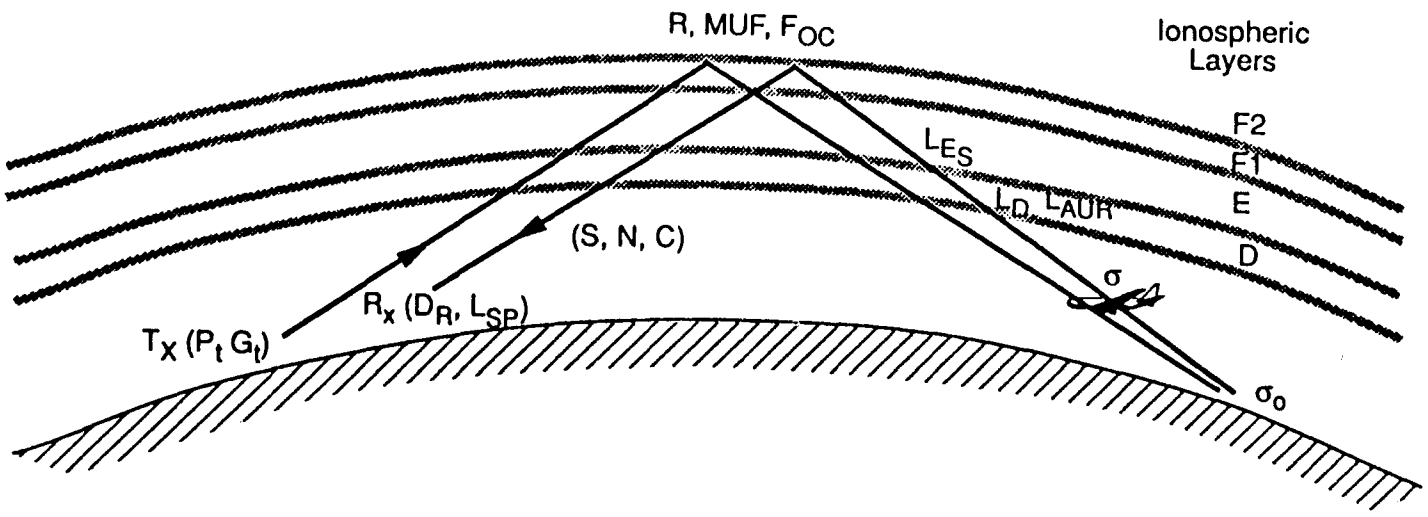

Figure 1. HFRAD OTH Radar Range Equation

we are not able to measure the individual loss terms, except perhaps the signal processing loss, if a calibration signal is available. The SNR of a target or the amplitude of peak surface return consists of a complicated interrelationship of radar, propagation, and ionospheric parameters. Hence, there are limitations in our ability to validate the various HFRAD model components.

From November 1990 through February 1991, MITRE was extensively involved in East Coast Radar System (ECRS) and West Coast Radar System (WCRS) data collection, processing, and analysis for the purpose of quantifying the operational performance of the ECRS and WCRS for single targets. The ECRS and WCRS database consists of radar, flight plan (assumed target position and velocity), and ionospheric measurements. Both the ECRS and WCRS measurements are associated either with aircraft that have been tracked and correlated, or with the mid-path location of the flight plan within the illuminated coverage area. In this paper we only present ECRS HFRAD/measurement results. All measured parameters are defined with respect to a coherent signal at the output of a single antenna element or at the input of a single receiver in units of dBm. In other words, the signal processing and receive array gain have been backed out of the measurement. Since the noise and clutter signals are assumed to be incoherent signals, the units are given in dBs (or scaled dB); the scaling factor, which is given by signal processing and receive array gains, needs to be calculated to convert dBs to dBm. For the AN/FPS-118 radar, the scaling factor is given approximately by

$$\begin{aligned} \textit{Scaling Factor } (S_F) &\approx CIT + ARG - L_{SP} \\ &\approx 3 + 19 - 8 = 14 \ dB \end{aligned}$$

where CIT is the radar waveform coherent integration time, ARG is the array receiver gain, and L_{SP} is the signal processing loss for a coherent signal.

The measured parameters are defined by the following:

SCV (dB) = Subclutter visibility. The ratio of the un-normalized surface return clutter peak to the background noise or transmitter-on noise level.

CLP (dBm) = Surface clutter peak.

TXN (dBs) = Transmitter-off noise. TXN is an incoherent signal, but is scaled as a coherent signal with respect to the output of a single antenna element.

BGN (dBs) = Transmitter-on noise. The sum of transmitter-off noise (TXN) plus spread-Doppler clutter (ICL), derived from the SCV and CLP measurements.

BNR (dB) = Background-to-noise ratio. Defined by the following expression

$$BNR = BGN - TXN\ (dB)$$

SNR (dB) = Median signal-to-noise ratio (SNR). Noise in SNR is referred to as transmitter-on noise. The median is computed from the first 15 hits after track establishment.

Measured radar waveform parameter definitions include the following:

Frequency (MHz) = Measured at time of TET or TMFP if no correlated track
PWBW (kHz) = Primary waveform bandwidth
PCIT (sec) = Primary waveform coherent integration time
PWRF (Hz) = Primary waveform repetition frequency
SWBW (kHz) = Secondary waveform bandwidth
SCIT (sec) = Secondary waveform coherent integration time
SWRF (Hz) = Secondary waveform repetition frequency

As noted earlier, hindcasting is expensive in terms of required analysis resources. For this reason, we selected only about 20 percent of the available ECRS data to be hindcast. This corresponds to hindcasting nine-day and seven-night ECRS missions (each mission corresponds to about a four-hour time interval). A hindcast day mission was defined to take place in the interval 1300-1900 Universal Time (UT), while a hindcast night mission took place from 0100-0400 UT. Only segment 1 (16.5 degrees to 76.5 degrees from true north) flight plan data was selected for the ECRS.

During the data collection period of November through February, the HFRAD-predicted radar frequency, ionospheric layer parameters, Kp, and SSN were very close to the monthly median values predicted by HFRAD. The geomagnetic conditions for that period were quiet to unsettled. Figure 2 shows a plot of the average daily and monthly Kp the filled diamonds show the ECRS hindcast days during November and December. The monthly average Kp is for November and December were about 2^- and 1^+, respectively. The daily average Kp for the hindcast missions varied from a maximum of about 3^+ to a low of about Kp = 1 with a mean of about Kp = 2^-. The ECRS hindcast missions represent a fairly broad sampling of day and night missions that includes periods of both good and poor radar performance.

Several program modifications were added to HFRAD to enable hindcasting capabilities such as user-specified radar frequency; user-specified ionospheric layer parameters (foF2, foF1, foE, foEs); user-specified foEs standard deviation (used in the sporadic-E signal loss integration computation); user-specified vertical incidence sounder location; and user- specified WRF (waveform repetition frequency).

The generation of environmental files includes the following information:

1. Radar operation frequency (MHz)
2. Ionospheric layer parameters (foF2, foF1, foE, foEs, in MHz)
3. Vertical incidence sounder location (geographic coordinates)
4. foEs standard deviation (MHz)
5. Geomagnetic activity (Kp)

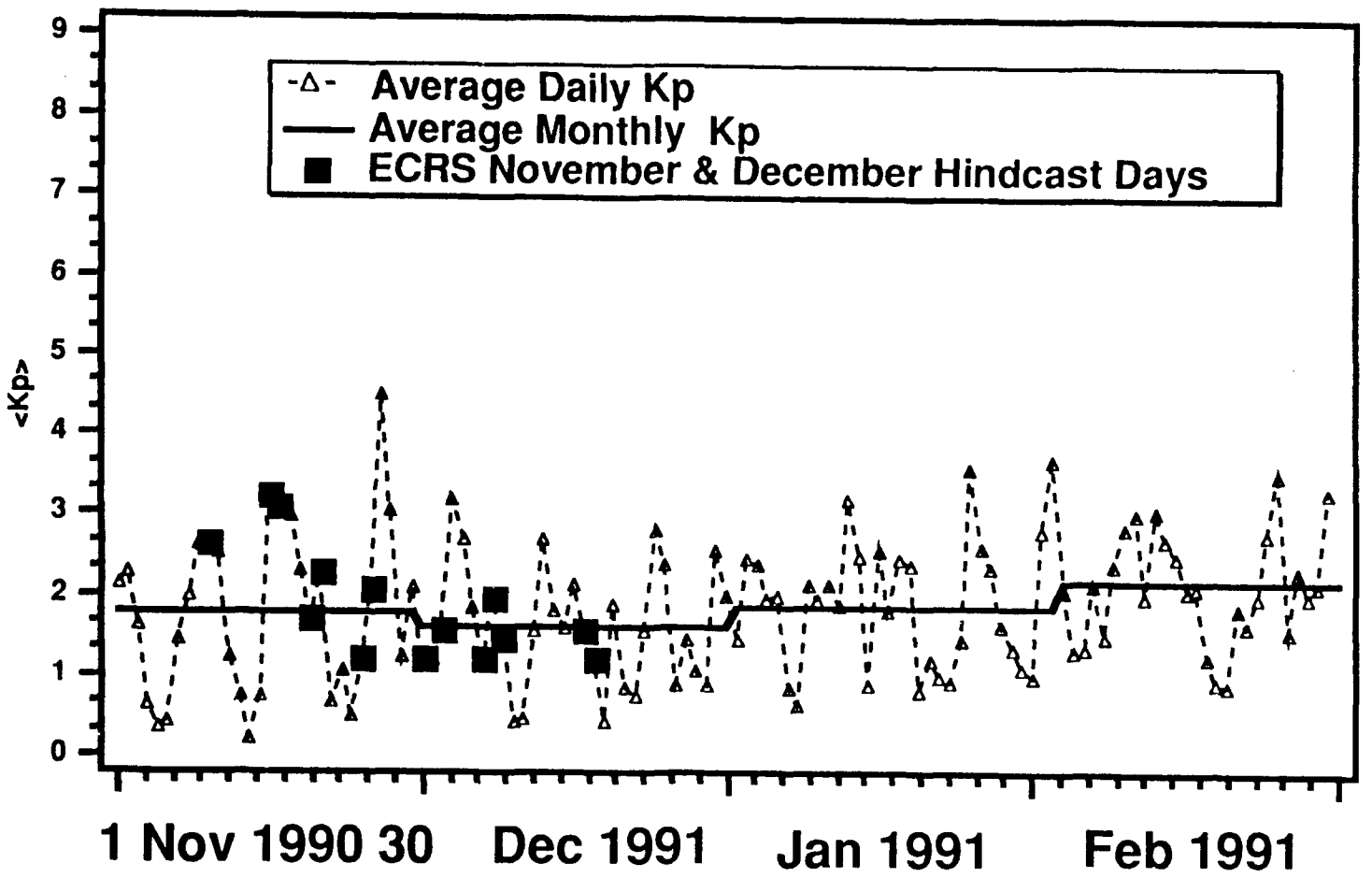

Figure 2. Plot of the Average Daily and Monthly Kp

6. Solar activity (SSN)
7. Time-of-day (local or Universal, in hours)
8. Month
9. Azimuth (degrees from True North)
10. Range start (km)
11. Range sampling interval (km)
12. Number of range intervals

Another important HFRAD hindcast input file is the radar file that includes the following information:

1. Transmitter power
3. Target radar cross section (large aircraft)
4. Target aspect angle
5. Target velocity
6. Radar waveform (CIT and bandwidth; WRF)

The measured, predictive, and measured-minus-predictive cumulative distributions of daytime and nighttime frequencies are shown in figure 3. The distribution curves tend to fall along several straight lines occurring with different break points in frequency. The daytime measured radar frequency distribution appears to be bimodal with a median daytime frequency of about 24.5 MHz and a standard deviation (based on the 84.9 percent point) of about 1.5 MHz. The predicted frequency distribution shows a bimodal shape similar to that of the measurement distribution plot, with a break point at 28 MHz corresponding to the radar's upper frequency limit. The meas-pred frequency distribution exhibits a complex bimodal shape, and it appears that HFRAD over-predicted the operating frequency by about 3 MHz. This may be related to the lack of available clear operating frequencies in the range of 26 to 28 MHz. The apparent bimodal shape of the distributions is, of course, strongly influenced by the truncation at the upper end of the frequency range. The nighttime frequency distributions have a much less noticeable break point, presumably because spectrum availability is more uniform and no equipment limitation exists, as is the case in

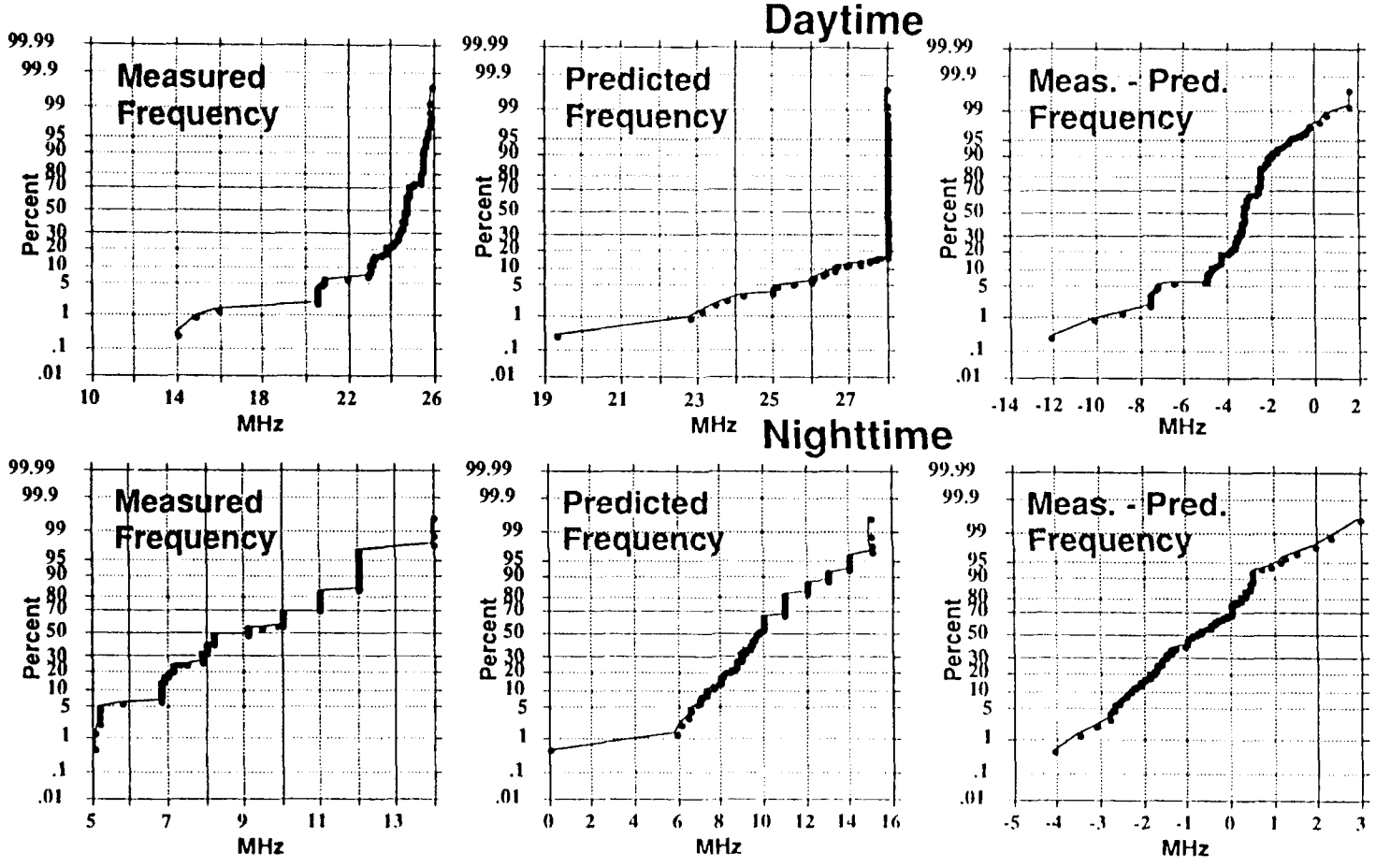

Figure 3. Cumulative Distributions of Daytime and Nighttime Frequencies

daytime. At night, the measured and predicted median frequencies were closer than in the daytime, with HFRAD predicting about 1 MHz higher than the measured median of 9 MHz.

Figures 4 and 5 show plots of daytime and nighttime ECRS measurements and HFRAD predictions (hindcast) of the sample size (number of flight plans), frequency, SCV, SNR, BNR, clutter peak, background noise, and TX-OFF as a function of azimuth. The HFRAD hindcast results were obtained by using the current baseline version of HFRAD. The sample size number represents the total number of measurements (i.e., flight plans) for a given segment. We used flight plans instead of "cases," since the number of flight plans per case varies with azimuth; the number of measurement samples is used in determining statistical significance. Note that the sample size increases from low azimuths to high azimuths, and it is larger in the daytime than at night, which is consistent with the flight plan data.

The measurements and HFRAD hindcast prediction comparisons of frequency suggest that the radars were operated nearly optimally (during both day and night in the case of the ECRS). As noted earlier, it appears, however, that some restriction existed on the upper frequency limit of the ECRS, perhaps related to spectral occupancy, which would have degraded daytime performance by ~1-2 dB. The azimuthal comparisons of the radar performance parameters (SCV, SNR, BNR, CLP, clutter, noise, etc.) show a strong azimuthal (or latitudinal) variation in the performance parameters. The largest differences appear to be associated with the HFRAD clutter model. They include the following:

1. HFRAD under-predicting clutter by about 1 to 4 dB in sectors 2, 5, 6, 7, and 8 in the daytime for ECRS

2. HFRAD over-predicting clutter by about 4 to 10 dB in segments 2, 3, and 4 and by about 1 to 4 dB in segments 5 through 8 in the nighttime for ECRS

These azimuthal clutter comparison results strongly suggest that the HFRAD clutter model still needs further improvement.

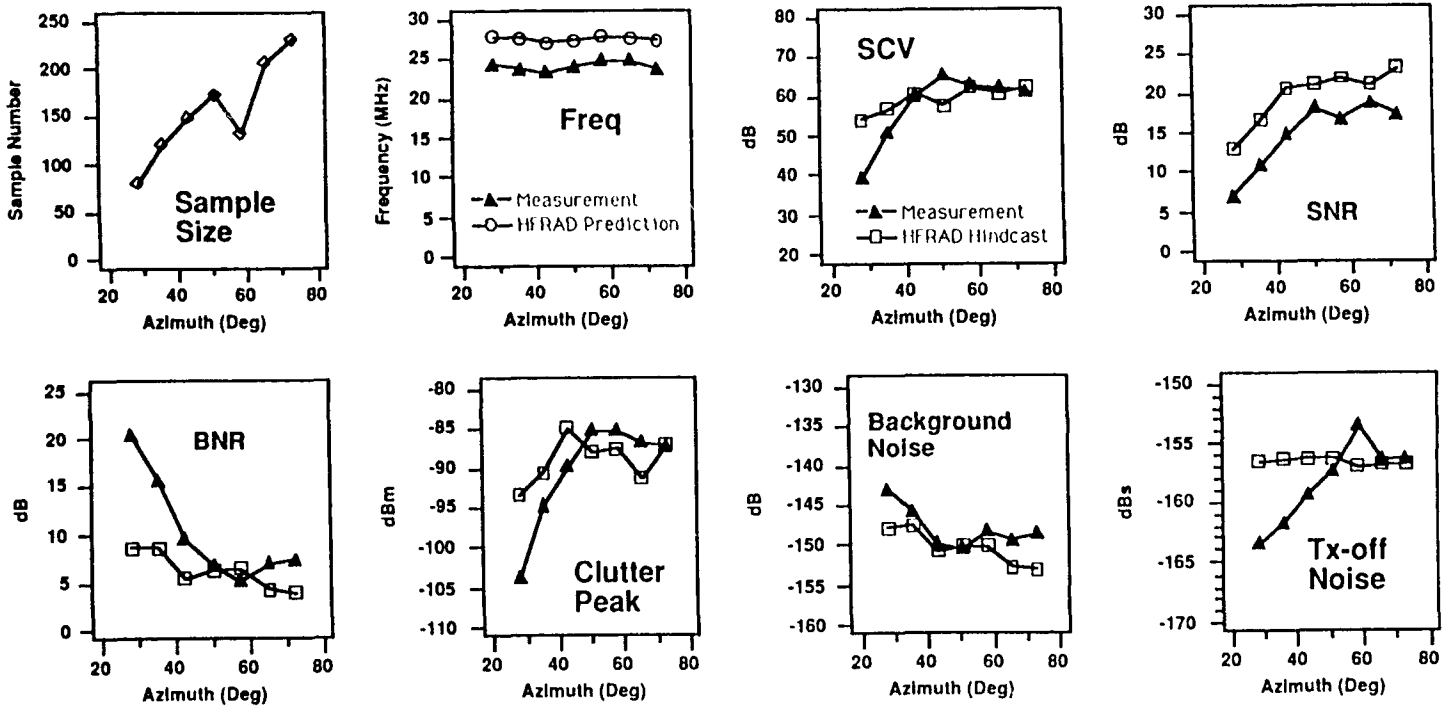

Figure 4. ECRS Daytime Hindcast HFRAD/Measurement Comparisons

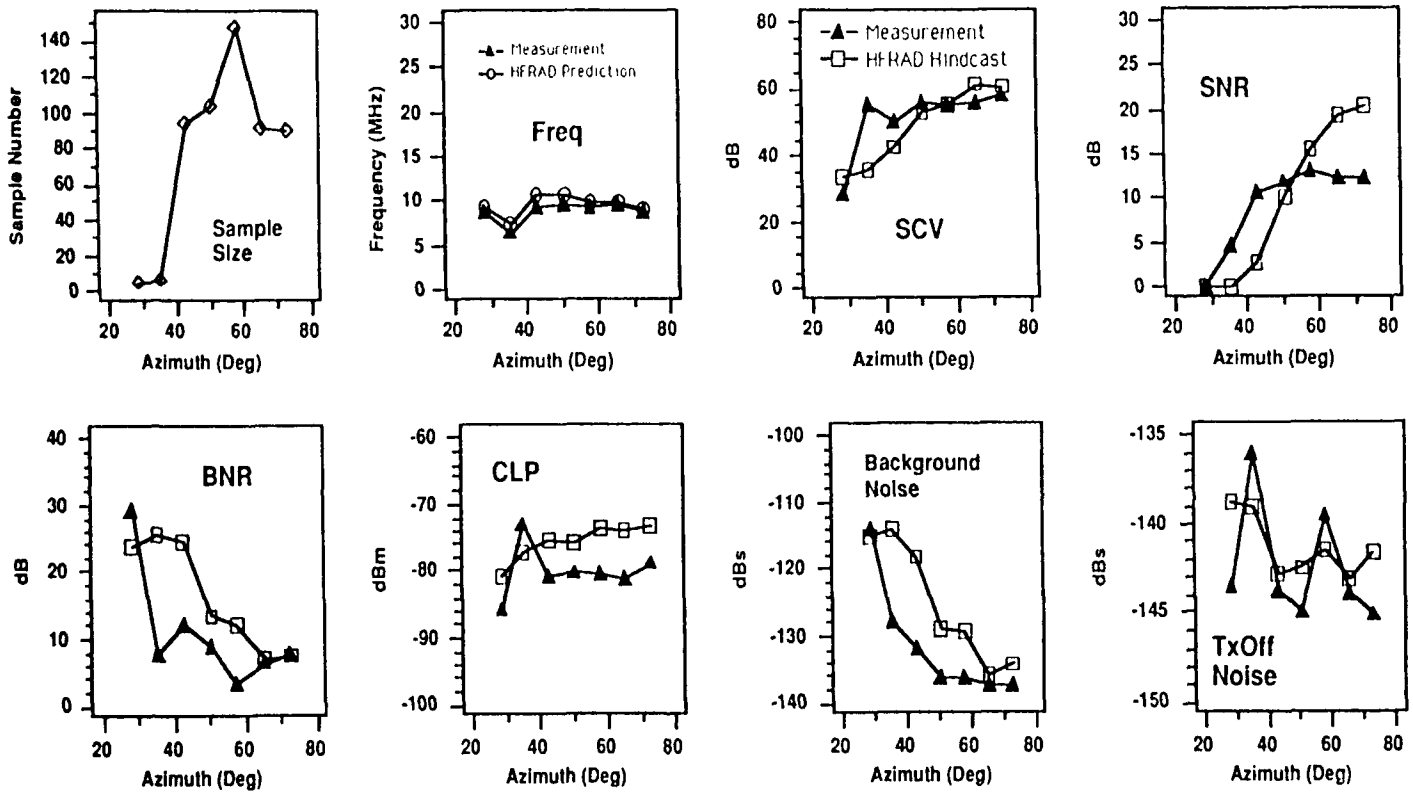

Figure 5. ECRS Nighttime Hindcast HFRAD/Measurement Comparisons

The noise model/measurement comparisons show fairly good agreement during the nighttime for the ECRS, but over-predict TX-OFF noise in sectors 2, 3, and 4 in the daytime. HFRAD under-predicts the daytime surface clutter peak (CLP) by about 3 dB in the more southerly sectors (i.e., 5-8) of ECRS segment 1, but it over-predicts CLP by about 10 dB in sector 2 of ECRS segment 1 during the daytime. This over-prediction of CLP may be attributed either to anomalous ionospheric absorption (i.e., winter anomaly or auroral absorption) or variability in surface reflectivity (i.e., sea ice instead of ocean water). At nighttime, the clutter CLP is over-predicted by about 5 dB in sectors 4 through 8.

An interesting comparison is the measurement-hindcast difference result. Figures 6 and 7 show the daytime and nighttime measurement-hindcast comparisons, respectively, as a function of azimuth. Also shown is the STDEV associated with the measurement-hindcast comparison. As may be anticipated, the measurement-hindcast comparison indicates closer agreement between measurement and HFRAD hindcast at azimuths greater than 40 degrees (lower latitudes), and poor agreement at the higher azimuths (less than 40 degrees). Note that the STDEV also appears larger at the more northerly azimuths (or higher latitudes).

The TX-OFF comparisons in figures 6 and 7 show that HFRAD tends to over-predict TX-OFF noise by about 3 dB at night and with the greatest STDEV at more northerly azimuths. The daytime comparisons show HFRAD over-predicting TX-OFF by as much as 7 dB at the higher latitudes (in ECRS sectors 2, 3, and 4), but show fairly good agreement for sectors 5 through 8. This suggests an azimuthal noise dependence, possibly related to man-made sources, that is not built into the International Radio Consultative Committee (CCIR) noise model (which is based on measurements with an antenna having an isotropic radiation pattern). It is also possible that auroral absorption, which is primarily a daytime phenomenon, is influencing the measured noise values.

In summary, the hindcasting technique permits separate model components to be isolated, to some extent, and is therefore a valuable aid in improving the accuracy of the overall performance model. By removing the uncertainty inherent in predicting the ionospheric structure prevailing during a radar measurement, as well as that associated with the selection of the radar operating frequency, hindcasting has been used in this paper to

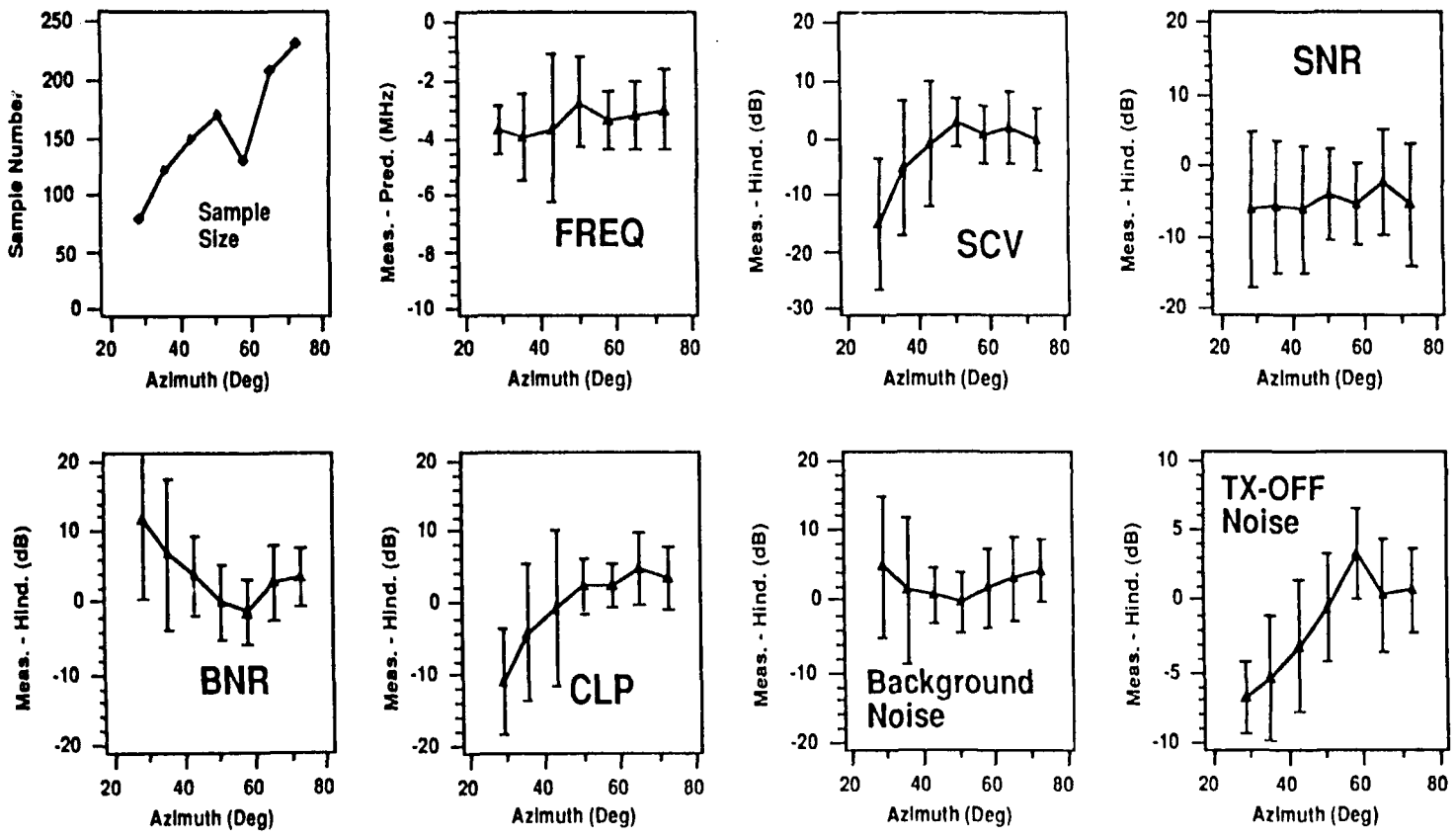

Figure 6. Mean of <Meas-Hindcast> for ECRS Daytime

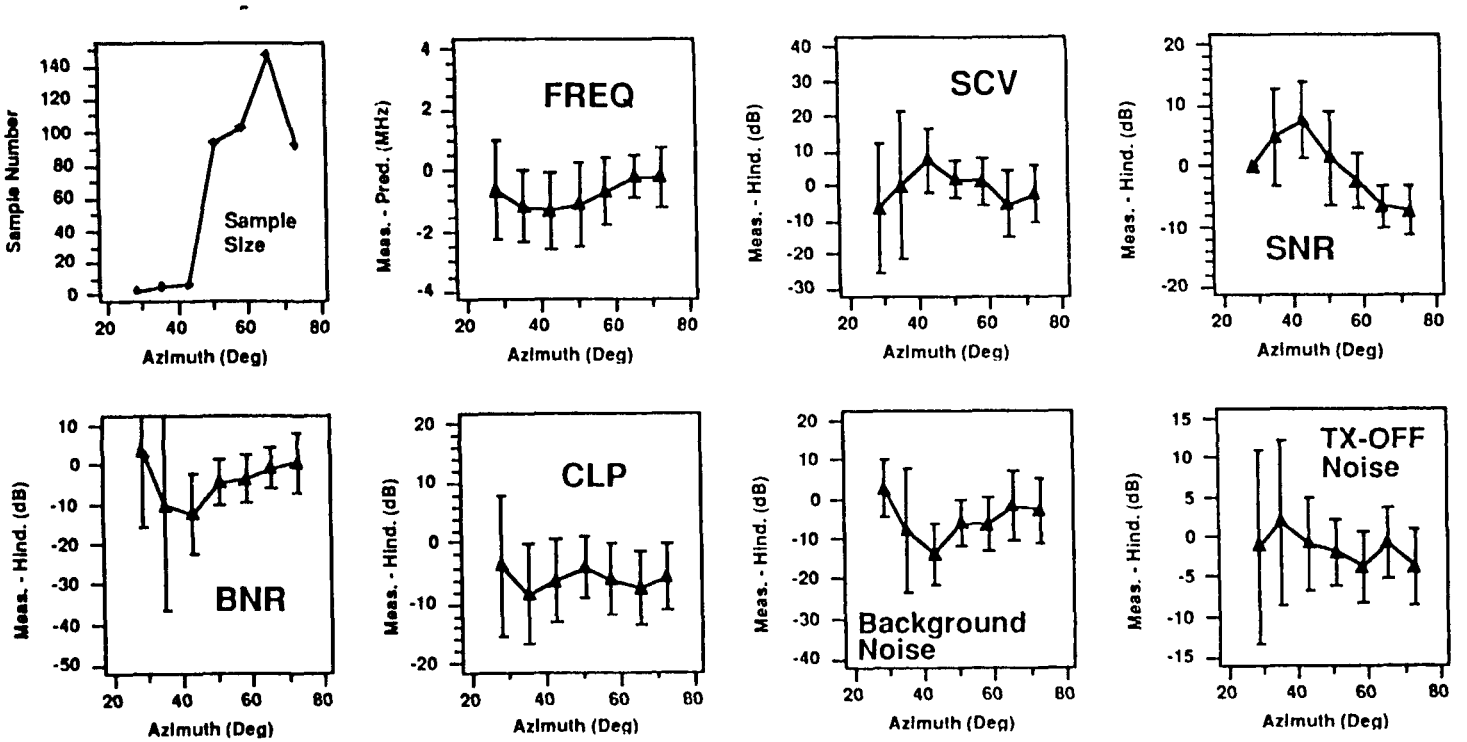

Figure 7. Mean of <Meas-Hindcast> for ECRS Nighttime

focus attention on the clutter, noise, and propagation loss components of HFRAD. It is recommended that further work be done in the areas of modeling Doppler-spread clutter, propagation loss, focusing, and noise modeling. In addition, it was recognized that the basic propagation model embodied in HFRAD should be improved to allow for inclusion of effects of horizontal gradients in the ionosphere.

DISTRIBUTION LIST

INTERNAL

A010

R. D. Haggarty
E. L. Key

A030

R. L. Fante
R. W. Jacobus

D010

E. J. Ferrari

D011

B. A. Deresh
W. I. Fenster

D050

J. W. Betz
E. A. Palo
B. D. Perry

D051

Y. Avniel
S. Dhar
S. D. O'Neil
R. Rifkin
R. P. Perry
S. A. Townes

D080

R. Wm. Bush
R. M. Davis
C. H. Gager
A. J. Goldberg
G. L. Guttrich
J. D. R. Kramer, Jr.
E. D. Ostroff

D080 (Concl'd)

J. Providakes (10)
G. W. Randig
J. M. Schoen
W. E. Sievers

D081

N. F. Doherty
J. E. Levy
R. C. Smith
A. L. Snyder
R. B. Young

D085

R. M. Coutts
L. M. DeRoeck
R. B. Godwin
S. N. Hunt
K. T. Kim
J. E. Kriegel
P. T. Lee
T. S. Lee
D. C. Miller
J. B. Moran
J. D. Moylan
K. R. Overfield
J. L. Pearlman
G. A. Robertshaw
K. B. Sarachik
J. C. Tang
L. J. Teig
N. M. Tomljanovich
L. D. Tromp
D. J. Violette
M. M. Weiner

D090

P. A. Bello

DISTRIBUTION LIST (CONCL'D)

D095

J. N. Freedman

G140

D. R. Uffelman

J103

D. H. Durkin

W090

T. J. Elkins (10)